Acta Cryst. (1998). A**54**, 129–136

Three-Beam Diffraction in Finite Perfect Crystals. II. Influence of Absorption, Resonant Scattering and Polarization

HELGE B. LARSEN AND GUNNAR THORKILDSEN*

Department of Mathematics and Natural Science, Stavanger College, Ullandhaug, 4004 Stavanger, Norway. E-mail: gunnar.thorkildsen@tn.his.no

(*Received 12 April 1997; accepted 13 August 1997*)

Abstract

By using the boundary-value Green-function technique, effects of absorption, resonant scattering and polarization are incorporated in the solution of the Takagi–Taupin equations for three-beam diffraction in finite perfect crystals. It is shown how such features may influence the dynamical interactions. The potential of three-beam interference acting as a phase-sensitive probe for resonant scattering is demonstrated. Depending on the applied model used for the calculations of the corrections to the atomic scattering factor, profile asymmetry reversal is theoretically predicted to occur near the photoelectric threshold in a finite germanium crystal. Significant distortions of the three-beam profiles are found for polarized incident radiation, especially for reflection triplets having an invariant phase sum near 90°.

1. Introduction

In the previous paper (Thorkildsen & Larsen, 1998), hereafter denoted TL-I, we presented a method for calculating azimuthal ψ curves for some *finite* crystal geometries based on the Takagi–Taupin equations. There we did not take into consideration resonant scattering, photoelectric absorption and polarization of the X-ray beams.

In elementary analysis, X-rays are considered to be scattered from free electrons. This is treated by applying the first Born approximation to the scattering system, yielding the atomic scattering factor, f. However, if the incident radiation is close to the frequency corresponding to an electronic transition of the scattering system, resonance phenomena become important. This gives a wavelength-dependent contribution to the scattering which also involves a phase shift. Such effects are normally dealt with using the second Born approximation, yielding the well known real (f') and imaginary (f'') corrections to the atomic scattering factor.

Photoelectric absorption is related to the imaginary part of the average electric susceptibility, χ_o. Its influence will depend upon the crystal shape and the diffraction geometry. Anomalous transmission, on the other hand, is related to the contribution from resonant scattering to the imaginary part of the coefficients, χ_h, building the Fourier series of the spatially varying electric susceptibility. It will affect the phase of the structure factors and thus the invariant triplet phase sum accessed in a three-beam diffraction experiment, making this a sensitive 'probe' for such features.

Resonant scattering effects will critically depend on the wavelength of the incident radiation.

Polarization, *i.e.* the vector nature of the waves constituting the displacement field, introduces an additional coupling between the amplitudes involved in three-beam diffraction. This may, however, be included in the formalism in a straightforward way. It has long been known that polarization complicates the phase-determination procedures in multiple diffraction experiments (Lipscomb, 1949). Several authors have investigated the effect using a kinematical approach (Moon & Shull, 1964; Caticha-Ellis, 1969; Prager, 1971; Cannata *et al.*, 1989) or plane-wave dynamical approaches (Juretschke, 1982*a*,*b*, 1984, 1986*a*,*b*; Chang & Tang, 1988; Luh & Chang, 1991; Weckert & Hümmer, 1997). The influence of polarization on multiple diffraction has also been verified and examined experimentally using conventional X-rays (Luh & Chang, 1991) and synchrotron radiation (Alexandropoulos *et al.*, 1990; Schwegle *et al.*, 1990). Another approach was adopted by Shen and co-workers (Shen & Finkelstein, 1990; Shen, 1993) who exploited three-beam diffraction to investigate the state of polarization of the incident beam.

2. Absorption

For the three-beam case, the Takagi–Taupin equations are written in the following form:

$$\begin{aligned} \partial\tilde{D}_o/\partial s_o &= i\kappa_{oh}\tilde{D}_h + i\kappa_{og}\tilde{D}_g \\ \partial\tilde{D}_h/\partial s_h &= i\kappa_{ho}\tilde{D}_o + i\kappa_{hg}\tilde{D}_g \\ \partial\tilde{D}_g/\partial s_g &= i\kappa_{go}\tilde{D}_o + i\kappa_{gh}\tilde{D}_h, \end{aligned} \tag{1}$$

where we at this stage neglect the polarization couplings. The amplitudes are transformed according to $p \in (o, h, g)$:

$$D_p(s_o, s_h, s_g) = \tilde{D}_p(s_o, s_h, s_g)\exp[2\pi i(\beta_h s_h + \beta_g s_g)]. \tag{2}$$

The definitions and nomenclature are all found in TL-I.

The solution of (1), with a point-source boundary condition on the entrance surface,

$$\tilde{D}_o^{(b)}(S) = \delta[s_h - s_h(S)]\,\delta[s_g - s_g(S)], \tag{3}$$

yields the Green functions we are searching for. We denote these by $(\tilde{d}_o, \tilde{d}_h, \tilde{d}_g)$. The actual boundary condition, continuity of **D** across the entrance surface, leads to the equation

$$\tilde{D}_o^{(b)}(S) = D_o^{(e)} \exp[-2\pi i \alpha_h s_h(S)] \exp[-2\pi i \alpha_g s_g(S)] \times \exp\{\pi i K \chi_o [s_o(S) + s_h(S) + s_g(S)]\}, \tag{4}$$

where $D_o^{(e)}$ is the amplitude associated with the incoming plane wave.

Photoelectric absorption and anomalous transmission are treated within the present formalism by introducing f' and f'' in the calculations for χ_o and χ_{p-q}. Anomalous transmission effects are included in the boundary-value Green functions, $\{\tilde{d}_p\}$, through the phases $\{\varphi_{pq}\}$.

The solution for the fields at a point, P, within the crystal is found by integration:

$$D_q(P) = JD_o^{(e)} \int \mathrm{d}S\, \tilde{d}_q(\Delta_o, \Delta_h, \Delta_g) \times \exp[2\pi i(\tilde{\alpha}_o \Delta_o + \tilde{\alpha}_h \Delta_h + \tilde{\alpha}_g \Delta_g)] \times \exp[-(\mu/2)(\Delta_o + \Delta_h + \Delta_g)], \tag{5}$$

where J is a geometrical factor (*cf.* TL-I) and $\Delta_q \equiv s_q(P) - s_q(S)$. We have also defined an effective excitation error that takes refraction into account:

$$\tilde{\alpha}_q = \alpha_q - K(\Re\chi_o/2). \tag{6}$$

μ is the linear photoelectric absorption coefficient, given by

$$\mu = -2\pi K \Im\chi_o, \tag{7}$$

where

$$\chi_o = -(r_e\lambda^2/\pi V_c)F_o. \tag{8}$$

Owing to the resonant scattering contribution,

$$|\kappa_{pq}| \neq |\kappa_{qp}| \tag{9}$$

$$\varphi_{pq} \neq -\varphi_{qp}. \tag{10}$$

The procedure of calculation is analogous to the one presented in TL-I and is carried out for the crystal geometries depicted in Figs. 1 and 2 of that paper.

The actual series expansions and surface integrations were performed using *MATHEMATICA*.† To ease the calculations, an elaborate coding scheme was adopted.

For the Laue–Laue case (Fig. 1 of TL-I), the result for the diffracted power to the third order is

$$\begin{aligned} P_h = P_L^0 \big(& g_1(\xi_o^i)\, g_2(\xi_h^r, \xi_h^i)\{1 - 2(|\eta_{hg}||\eta_{go}|/|\eta_{ho}|) \\ & \times [g_4(\xi_g^r, \xi_g^i)\cos(\varphi_\Sigma - \varphi_x) \\ & + g_3(\xi_g^r, \xi_g^i)\sin(\varphi_\Sigma - \varphi_x)]\} \\ & + (|\eta_{hg}|^2|\eta_{go}|^2/|\eta_{ho}|^2) g_1(\xi_o^i) g_5(\xi_g^r, \xi_g^i) g_2(\xi_h^r, \xi_h^i) \\ & + 2|\eta_{go}||\eta_{og}| g_6(\xi_o^i) g_2(\xi_h^r, \xi_h^i)[-g_3(\xi_g^r, \xi_g^i)\cos\varphi_y \\ & + g_4(\xi_g^r, \xi_g^i)\sin\varphi_y] + 2|\eta_{gh}||\eta_{hg}| g_1(\xi_o^i) \\ & \times \{[g_4(\xi_g^r, \xi_g^i) g_8(\xi_h^r, \xi_h^i) - g_3(\xi_g^r, \xi_g^i) g_7(\xi_h^r, \xi_h^i)]\cos\varphi_z \\ & + [g_4(\xi_g^r, \xi_g^i) g_7(\xi_h^r, \xi_h^i) \\ & + g_3(\xi_g^r, \xi_g^i) g_8(\xi_h^r, \xi_h^i)]\sin\varphi_z\}\big), \end{aligned} \tag{11}$$

whereas, for the Bragg–Laue case (Fig. 2 of TL-I),

$$\begin{aligned} P_h = P_B^0 \big(& g_9(\xi_h^r, \xi_h^i)\{1 - 2(|\eta_{hg}||\eta_{go}|/|\eta_{ho}|) \\ & \times [g_4(\xi_g^r, \xi_g^i)\cos(\varphi_\Sigma - \varphi_x) \\ & + g_3(\xi_g^r, \xi_g^i)\sin(\varphi_\Sigma - \varphi_x)]\} \\ & + (|\eta_{hg}|^2|\eta_{go}|^2/|\eta_{ho}|^2) g_5(\xi_g^r, \xi_g^i) g_9(\xi_h^r, \xi_h^i) \\ & + 2|\eta_{go}||\eta_{og}|\{[g_4(\xi_g^r, \xi_g^i) g_{10}(\xi_h^r, \xi_h^i) \\ & - g_3(\xi_g^r, \xi_g^i) g_{11}(\xi_h^r, \xi_h^i)]\cos\varphi_y + [g_3(\xi_g^r, \xi_g^i) g_{10}(\xi_h^r, \xi_h^i) \\ & + g_4(\xi_g^r, \xi_g^i) g_{11}(\xi_h^r, \xi_h^i)]\sin\varphi_y\} \\ & + 2|\eta_{gh}||\eta_{hg}|\{[g_4(\xi_g^r, \xi_g^i) g_{10}(\xi_h^r, \xi_h^i) \\ & - g_3(\xi_g^r, \xi_g^i) g_{11}(\xi_h^r, \xi_h^i)]\cos\varphi_z \\ & + [g_3(\xi_g^r, \xi_g^i) g_{10}(\xi_h^r, \xi_h^i) \\ & + g_4(\xi_g^r, \xi_g^i) g_{11}(\xi_h^r, \xi_h^i)]\sin\varphi_z\}\big). \end{aligned} \tag{12}$$

In equations (11) and (12), the contribution to primary extinction is omitted – *i.e.* terms proportional to $|\eta_{ho}|^2$. $\xi_q^r = 2\pi\tilde{\alpha}_q l_q$, $2\xi_q^i = \mu l_q$, whereas the triplet invariant phase sum is given by $\varphi_\Sigma = \varphi_{oh} + \varphi_{hg} + \varphi_{go}$. We have defined $\varphi_x = \varphi_{oh} + \varphi_{ho}$, $\varphi_y = \varphi_{og} + \varphi_{go}$, $\varphi_z = \varphi_{gh} + \varphi_{hg}$ and finally $|\eta_{pq}| = |\kappa_{pq}| l_p$. Note that the experimental phase sum appears in the combination $\varphi_\Sigma - \varphi_x = \varphi_{hg} + \varphi_{go} - \varphi_{ho}$. $P_{L,B}^0$ represent the kinematical two-beam power in each case. The functions $\{g_i\}$ are

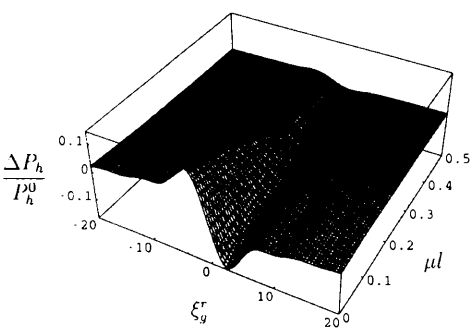

Fig. 1. Effect of increasing absorption. Isotropic crystal shape; $l_o = l_h = l_g = l$. Laue–Laue scattering geometry. Invariant triplet phase sum: $\varphi_\Sigma = 0°$.

† *MATHEMATICA* is a trademark for Wolfram Research Inc., Champaign, IL 61820, USA.

given in Appendix *A*. Calculations have been performed up to the fourth order and these results are used for generating Figs. 1, 2 and 3.

The effect of absorption on a three-beam ψ profile is shown in Fig. 1 for an isotropic crystal ($l_o = l_h = l_g = l$). We see how the dynamical perturbations are damped out as μl increases, *i.e.* as absorption becomes more pronounced.

3. Resonant scattering

The 'phase sensitivity' of three-beam diffraction is exploited in order to investigate resonant scattering near the photoelectric threshold in germanium. We have compared different anomalous-scattering-factor models used for calculations of $f'(\lambda)$ and $f''(\lambda)$; the one by Cromer & Liberman, which utilizes the dipole approximation (Cromer & Liberman, 1970, 1981; Cromer, 1995), and that introduced more recently by Kissel and co-workers (Kissel *et al.*, 1980, 1995; Kissel, 1995). The latter model is based on second-order scattering-matrix theory in which many-body effects have been taken into account.

Using equations (11) and (12), we have calculated ψ curves at four different wavelengths for the (115)(220)($\bar{1}\bar{1}5$) reflection triplet in germanium. Here, $h = (115)$ denotes the primary reflection, whereas $g = (220)$ and $h - g = (\bar{1}\bar{1}5)$ are the secondary and coupling reflections, respectively. In order to get valid input parameters for the series-expansion solution, the calculations are carried out for a very small model crystal: $l_o = l_h = l_g = 1$ μm. Both Laue–Laue and Bragg–Laue scattering were considered. Calculated phase sums for the various wavelengths and different anomalous-scattering-factor models are given in Tables 1 and 2.

Table 1. *Calculated phase sums for various wavelengths using Cromer & Liberman's model for resonant scattering parameters*

Reflection triplet: (115)(220)($\bar{1}\bar{1}5$).

λ (Å)	1.0000	1.1165	1.1166	1.1211	1.2000
φ_Σ (°)	30	66	13	6.2	6.0
$\varphi_x = \varphi_z$ (°)	22	51	10	4.6	4.3
$\varphi_\Sigma - \varphi_x$ (°)	8.0	15	3.0	1.6	1.7
φ_y (°)	16	30	5.0	3.1	3.0

It should be noted that the models predict the threshold at slightly different energies. The photoelectric threshold for Ge should, according to the Cromer–Liberman model, be at $\lambda = \lambda_K = 1.11659$ Å, whereas the Kissel model gives $\lambda_K = 1.12105$ Å.

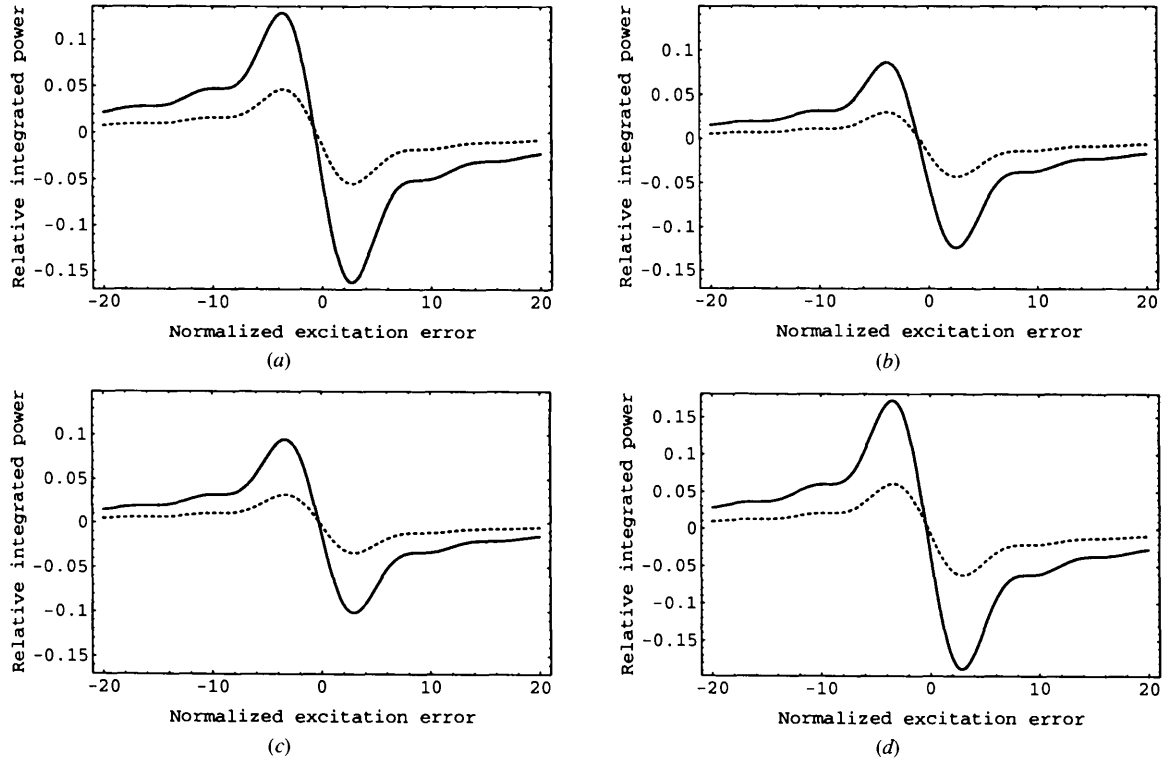

Fig. 2. Simulated ψ profiles for the germanium (115)(220)($\bar{1}\bar{1}5$) triplet at various wavelengths. $l_o = l_h = l_g = 1$ μm. Resonant scattering parameters after Cromer & Liberman. Solid line: Laue–Laue case; dashed line: Bragg–Laue case. (*a*) $\lambda = 1.0000$ Å; (*b*) $\lambda = 1.1165$ Å; (*c*) $\lambda = 1.1166$ Å; (*d*) $\lambda = 1.2000$ Å.

Table 2. *Calculated phase sums for various wavelengths using Kissel et al.'s model for resonant scattering parameters*

Reflection triplet: (115)(220)($\bar{1}\bar{1}5$).

λ (Å)	1.0000	1.1165	1.1210	1.1211	1.2000
φ_Σ (°)	33	49	150	27	6.6
$\varphi_x = \varphi_z$ (°)	25	38	−8.3	23	5.0
$\varphi_\Sigma - \varphi_x$ (°)	8.0	11	160	4.0	1.6
φ_y (°)	17	23	−41	6.5	3.2

In Figs. 2 and 3, the resulting ψ profiles for four different wavelengths are shown for both the Laue–Laue and Bragg–Laue cases. We note the shift in the overall level of dynamical perturbation of the two-beam power for the primary reflection (115) in the two cases. This is mainly due to different absorption effects. Furthermore, the perturbation decreases as the threshold is approached from the high-energy side. Using the Kissel model, we get a complete reversal of the asymmetry near the edge (Fig. 3*c*). This is not found using the Cromer–Liberman model. Such a reversal has been experimentally observed (Larsen, 1997) and will be the subject of a following paper (Thorkildsen *et al.*, 1998). On the low-energy side of the edge, we have qualitative similarity (Figs. 2*c* and 3*c*) and, for wavelengths far from the threshold, the ψ curves obtained using the different models for calculating f' and f'' are in practice identical.

4. Polarization

By assigning polarization vectors ($\hat{\boldsymbol{\sigma}}_p$ and $\hat{\boldsymbol{\pi}}_p$; $p \in \{o, g, h\}$) to the Laue–Laue case, as shown in Fig. 1 of TL-I, such that $\hat{\mathbf{s}}_p$, $\hat{\boldsymbol{\sigma}}_p$ and $\hat{\boldsymbol{\pi}}_p$ form a Cartesian base, we may write the Takagi–Taupin equations for a three-beam case in the following way:

$$\begin{aligned}
\partial\tilde{D}_o^\sigma/\partial s_o &= i\kappa_{oh}^{\sigma\sigma}\tilde{D}_h^\sigma + i\kappa_{og}^{\sigma\sigma}\tilde{D}_g^\sigma \\
\partial\tilde{D}_o^\pi/\partial s_o &= i\kappa_{oh}^{\pi\pi}\tilde{D}_h^\pi + i\kappa_{og}^{\pi\pi}\tilde{D}_g^\pi + i\kappa_{og}^{\pi\sigma}\tilde{D}_g^\sigma \\
\partial\tilde{D}_h^\sigma/\partial s_h &= i\kappa_{ho}^{\sigma\sigma}\tilde{D}_o^\sigma + i\kappa_{hg}^{\sigma\sigma}\tilde{D}_g^\sigma \\
\partial\tilde{D}_h^\pi/\partial s_h &= i\kappa_{ho}^{\pi\pi}\tilde{D}_o^\pi + i\kappa_{hg}^{\pi\pi}\tilde{D}_g^\pi + i\kappa_{hg}^{\pi\sigma}\tilde{D}_g^\sigma \\
\partial\tilde{D}_g^\sigma/\partial s_g &= i\kappa_{go}^{\sigma\sigma}\tilde{D}_o^\sigma + i\kappa_{go}^{\sigma\pi}\tilde{D}_o^\pi + i\kappa_{gh}^{\sigma\sigma}\tilde{D}_h^\sigma + i\kappa_{gh}^{\sigma\pi}\tilde{D}_h^\pi \\
\partial\tilde{D}_g^\pi/\partial s_g &= i\kappa_{go}^{\pi\pi}\tilde{D}_o^\pi + i\kappa_{gh}^{\pi\pi}\tilde{D}_h^\pi.
\end{aligned} \tag{13}$$

The transformation $D_p^\tau = \tilde{D}_p^\tau \exp(2\pi i \sum_q \beta_q s_q)$, $\tau \in \{\sigma, \pi\}$, *cf.* equation (2), is applied individually to each of the six amplitudes of equation (13). In this part, we do not take absorption into consideration. The unit polarization vectors are chosen such that the $\hat{\boldsymbol{\pi}}$ components are in the plane spanned by ($\hat{\mathbf{s}}_o$, $\hat{\mathbf{s}}_h$). Within this

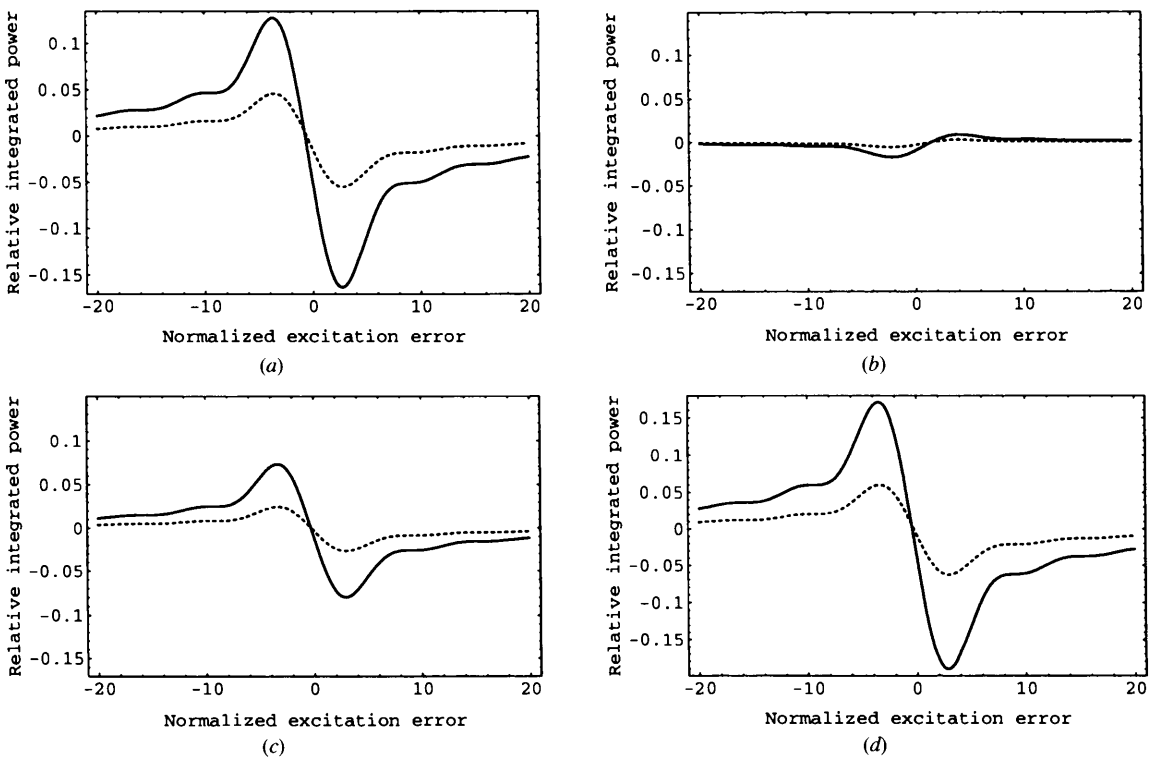

Fig. 3. Simulated ψ profiles for the germanium (115)(220)($\bar{1}\bar{1}5$) triplet at various wavelengths. $l_o = l_h = l_g = 1$ µm. Resonant scattering parameters after Kissel *et al.*. Solid line: Laue–Laue case; dashed line: Bragg–Laue case. (*a*) $\lambda = 1.0000$ Å; (*b*) $\lambda = 1.1210$ Å; (*c*) $\lambda = 1.1211$ Å; (*d*) $\lambda = 1.2000$ Å.

reference frame $\hat{\boldsymbol{\sigma}}_o \cdot \hat{\boldsymbol{\pi}}_h = \hat{\boldsymbol{\sigma}}_h \cdot \hat{\boldsymbol{\pi}}_o = \hat{\boldsymbol{\sigma}}_o \cdot \hat{\boldsymbol{\pi}}_g = \hat{\boldsymbol{\sigma}}_h \cdot \hat{\boldsymbol{\pi}}_g = 0$ and $\hat{\boldsymbol{\sigma}}_o \cdot \hat{\boldsymbol{\sigma}}_h = 1$. The remaining couplings are included in the calculations through the parameters $\kappa_{pq}^{\tau\nu}$ [equation (6) of TL-I]. We also define, restricting the discussion to symmetrical scattering:

$$\begin{aligned} |\hat{\boldsymbol{\pi}}_o \cdot \hat{\boldsymbol{\pi}}_h| &= c_1 \\ |\hat{\boldsymbol{\pi}}_o \cdot \hat{\boldsymbol{\pi}}_g| &= |\hat{\boldsymbol{\pi}}_h \cdot \hat{\boldsymbol{\pi}}_g| = c_2 \\ |\hat{\boldsymbol{\sigma}}_o \cdot \hat{\boldsymbol{\sigma}}_g| &= |\hat{\boldsymbol{\sigma}}_h \cdot \hat{\boldsymbol{\sigma}}_g| = c_3 \\ |\hat{\boldsymbol{\sigma}}_g \cdot \hat{\boldsymbol{\pi}}_o| &= |\hat{\boldsymbol{\sigma}}_g \cdot \hat{\boldsymbol{\pi}}_h| = c_4. \end{aligned} \tag{14}$$

Expressions for the trigonometric factors $\{c_i\}$ are given in Appendix A.

The solution of (13) is found by introducing a linear operator, $\mathcal{L}_{pq}^{\tau\nu}$, similar to equation (11) of TL-I, in which the polarization couplings are included:

$$\mathcal{L}_{pq}^{\tau\nu} \tilde{D}_q^{\nu}(s_o, s_h, s_g) = i\kappa_{pq}^{\tau\nu} \int_{s_p^b}^{s_p} \mathrm{d}s_p' \, \tilde{D}_q^{\nu}(s_p', \{s_q\}) \tag{15}$$

and applying the boundary conditions [equation (13) of TL-1] to each state of polarization. The calculations for the Laue–Laue (and Bragg–Laue) case still follows the procedure presented in TL-I. The algebraic expressions for the coefficients in the series expansion of the diffracted power, P_h, grow very rapidly and in this case calculations up to the third order are performed – *i.e.* the first correction† to the term carrying the phase information is found.

The result is presented below for the Laue–Laue case:

$$\begin{aligned} P_h = (c/2\varepsilon_0)(v_L/l_o)\big(&2(D_{0\pi}^2|\eta_{oh}^{\pi\pi}|^2 + D_{0\sigma}^2|\eta_{oh}^{\sigma\sigma}|^2) f_1(\xi_h) \\ &- 4(D_{0\pi}^2|\eta_{gh}^{\pi\pi}||\eta_{og}^{\pi\pi}||\eta_{oh}^{\pi\pi}| + D_{0\pi}^2|\eta_{gh}^{\sigma\pi}||\eta_{og}^{\pi\sigma}||\eta_{oh}^{\pi\pi}| \\ &+ D_{0\pi}D_{0\sigma}|\eta_{gh}^{\sigma\pi}||\eta_{og}^{\sigma\sigma}||\eta_{oh}^{\pi\pi}| \\ &+ D_{0\pi}D_{0\sigma}|\eta_{gh}^{\sigma\sigma}||\eta_{og}^{\pi\sigma}||\eta_{oh}^{\sigma\sigma}| \\ &+ D_{0\sigma}^2|\eta_{gh}^{\sigma\sigma}||\eta_{og}^{\sigma\sigma}||\eta_{oh}^{\sigma\sigma}|)\{f_2(\xi_g)\cos\varphi_\Sigma \\ &+ f_1(\xi_g)\sin\varphi_\Sigma\} f_1(\xi_h) - (D_{0\pi}^2|\eta_{oh}^{\pi\pi}|^4 \\ &+ D_{0\sigma}^2|\eta_{oh}^{\sigma\sigma}|^4) f_1(\xi_h) - 2\{D_{0\pi}(D_{0\pi}|\eta_{og}^{\pi\pi}|^2 \\ &+ D_{0\pi}|\eta_{og}^{\pi\sigma}|^2 + D_{0\sigma}|\eta_{og}^{\pi\sigma}||\eta_{og}^{\sigma\sigma}|)|\eta_{oh}^{\pi\pi}|^2 \\ &- D_{0\sigma}(D_{0\pi}|\eta_{og}^{\pi\sigma}| + D_{0\sigma}|\eta_{og}^{\sigma\sigma}|)|\eta_{oh}^{\sigma\sigma}|^2|\eta_{og}^{\sigma\sigma}|\} \\ &\times f_1(\xi_g) f_1(\xi_h) + 4\{(D_{0\pi}|\eta_{og}^{\pi\sigma}| + D_{0\sigma}|\eta_{og}^{\sigma\sigma}|)^2|\eta_{gh}^{\sigma\sigma}|^2 \\ &+ (D_{0\pi}|\eta_{gh}^{\pi\pi}||\eta_{og}^{\pi\pi}| + D_{0\sigma}|\eta_{gh}^{\sigma\pi}||\eta_{og}^{\pi\sigma}| \\ &+ D_{0\sigma}|\eta_{gh}^{\sigma\pi}||\eta_{og}^{\sigma\sigma}|)^2\} f_3(\xi_g) f_1(\xi_h) \\ &- 4\{D_{0\sigma}|\eta_{gh}^{\sigma\sigma}||\eta_{oh}^{\sigma\sigma}|(D_{0\pi}|\eta_{gh}^{\sigma\pi}||\eta_{oh}^{\pi\pi}| \\ &+ D_{0\sigma}|\eta_{gh}^{\sigma\sigma}||\eta_{oh}^{\sigma\sigma}|) + D_{0\pi}|\eta_{oh}^{\pi\pi}|(D_{0\pi}|\eta_{gh}^{\pi\pi}|^2|\eta_{oh}^{\pi\pi}| \\ &+ D_{0\pi}|\eta_{gh}^{\sigma\pi}|^2|\eta_{oh}^{\pi\pi}| + D_{0\sigma}|\eta_{gh}^{\sigma\pi}||\eta_{gh}^{\sigma\sigma}||\eta_{oh}^{\sigma\sigma}|)\} \\ &\times \{f_1(\xi_g) f_1(\xi_h) + f_2(\xi_g) f_4(\xi_h)\}\big). \end{aligned}$$

† Terms corresponding to *Umweganregung* and *Aufhellung*.

$D_{0\sigma,\pi}$ represent the strength of the incoming wave associated with each state of polarization and $|\eta_{pq}^{\tau\nu}| = |\kappa_{pq}^{\tau\nu}|(l_p l_q)^{1/2}$. The functions $\{f_i\}$ are the same as given in equation (32) in TL-I; they are also tabulated in Appendix A for the sake of completeness. v_L is the volume of the crystal (Fig. 1 of TL-I), ε_0 is the permittivity of vacuum and c the speed of light.

It is clear that a pure σ- (or π-) polarized incoming wave may generate both σ- and π-polarized wave fields within the crystal. This is consistent with the findings of Chang & Tang (1988) who used standard plane-wave theory.

By explicitly writing the geometrical coupling factors inherent in the $\eta_{pq}^{\tau\nu}$ parameters, we may express the relative change in the *integrated* power in the same fashion as equation TL-I (34):

$$\begin{aligned} \Delta\mathcal{P}_h(\xi_g)/\mathcal{P}_h^o = &-2(|\eta_{hg}||\eta_{go}|/|\eta_{ho}|)p_1[f_2(\xi_g)\cos\varphi_\Sigma \\ &+ f_1(\xi_g)\sin\varphi_\Sigma] - (|\eta_{hg}|^2 p_2 + |\eta_{go}|^2 p_3) \\ &\times f_1(\xi_g) + 2(|\eta_{hg}|^2|\eta_{go}|^2/|\eta_{ho}|^2)\, p_4 f_3(\xi_g), \end{aligned} \tag{16}$$

where the 'polarization factors', $\{p_i\}$, are given by

$$\begin{aligned} p_1 &= b_\sigma^2 c_3^2 + b_\sigma b_\pi c_3 c_4(1 + c_1) + b_\pi^2 c_1(c_2^2 + c_4^2) \\ p_2 &= b_\sigma^2 c_3^2 + 2b_\sigma b_\pi c_1 c_3 c_4 + b_\pi^2 c_1^2(c_2^2 + c_4^2) \\ p_3 &= b_\sigma^2 c_3^2 + b_\sigma b_\pi c_3 c_4(1 + c_1^2) + b_\pi^2 c_1^2(c_2^2 + c_4^2) \\ p_4 &= b_\sigma^2(c_3^4 + c_4^4 + c_3^2 c_4^2 + 2c_3 c_4^3) + 2b_\sigma b_\pi(c_3^3 c_4 + c_2^2 c_4^2 \\ &\quad + c_2^2 c_3 c_4) + b_\pi^2(c_3^2 c_4^2 + c_2^4) \end{aligned}$$

with $\{c_i\}$ defined in (14) and

$$\begin{aligned} b_\sigma^2 &= |D_{0\sigma}|^2/(|D_{0\sigma}|^2 + |D_{0\pi}|^2) \\ b_\sigma b_\pi &= |D_{0\sigma}||D_{0\pi}|/(|D_{0\sigma}|^2 + |D_{0\pi}|^2) \\ b_\pi^2 &= |D_{0\pi}|^2/(|D_{0\sigma}|^2 + |D_{0\pi}|^2). \end{aligned}$$

We see that the only difference between TL-I (34) and (16) is the presence of the polarization factors in the latter. They serve as geometrical 'weighting factors', caused by the coupling between the wave fields excited and the state of polarization of the incident beam. Depending on their relative contribution, the correct profile asymmetry may be extinguished, making interpretation difficult (Juretschke, 1982*b*, 1984, 1986*a*). It has been pointed out (Weckert & Hümmer, 1997) that a complete three-beam profile asymmetry reversal can occur if some of the scalar products between the polarization vectors change signs due to geometrical reasons. For the present finite model crystal, the scattering geometry is to a certain extent fixed, thereby restricting the polarization vectors within the chosen frame. The calculations nevertheless show that the effects of polarization on three-beam azimuthal ψ-scan profiles may be significant and the predictions from the present

theory seem to be in keeping with experimental results found in the literature (Luh & Chang, 1991; Schwegle *et al.*, 1990). In Figs. 4 and 5, the relative change in the integrated power, as a function of both φ_Σ and $\xi_g(\psi)$, for different types of incident-beam polarization, is shown. In Fig. 4, we have a case of a strong primary and secondary reflection and a weak coupling. Fig. 5 simulates a case of a weak primary reflection and strong secondary and coupling reflections.

It is seen that the unpolarized beam yields the highest peak power in the maps and that a polarized incoming beam may cause anomalities, leading to problems of interpreting the ψ curves. This is evident especially in cases where φ_Σ is near 90°, using for instance the scheme of Hümmer & Weckert (1994). Such features occur both for a σ-polarized incoming beam (*cf.* Fig. 4) and for a π-polarized beam (*cf.* Fig. 5). Similar results are also (qualitatively) obtained for the Bragg–Laue case.

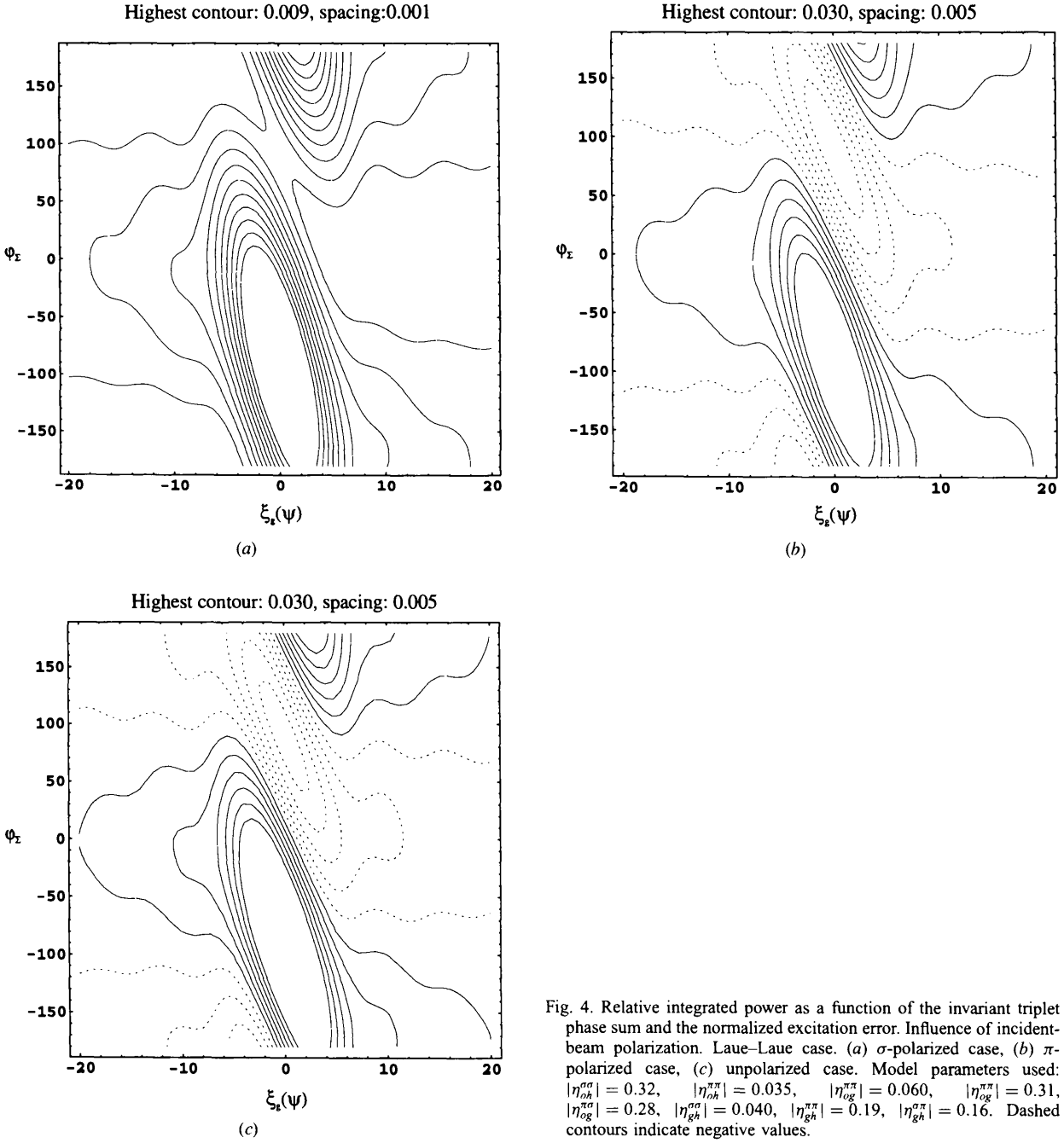

Fig. 4. Relative integrated power as a function of the invariant triplet phase sum and the normalized excitation error. Influence of incident-beam polarization. Laue–Laue case. (*a*) σ-polarized case, (*b*) π-polarized case, (*c*) unpolarized case. Model parameters used: $|\eta_{oh}^{\sigma\sigma}| = 0.32$, $|\eta_{oh}^{\pi\pi}| = 0.035$, $|\eta_{og}^{\pi\pi}| = 0.060$, $|\eta_{og}^{\pi\pi}| = 0.31$, $|\eta_{og}^{\pi\sigma}| = 0.28$, $|\eta_{gh}^{\sigma\sigma}| = 0.040$, $|\eta_{gh}^{\pi\pi}| = 0.19$, $|\eta_{gh}^{\sigma\pi}| = 0.16$. Dashed contours indicate negative values.

5. Conclusions

This paper shows how absorption/resonant scattering and polarization couplings may be treated for three-beam diffraction in finite crystals using the Takagi–Taupin equations.

In the case of resonant scattering, the value of the invariant triplet phase sum, φ_Σ, and hence the shape of the ψ profile, strongly depends upon the values of f' and f''. The Kissel model, which we have used for some of our calculations, shows severe resonant effects near the photo-electric threshold leading to a shift in the phase sum of $\sim 180°$. The large values of f' based on this model (*cf.* Table 2) may be unrealistically high but the calculations nevertheless show that three-beam diffraction can be used as a sensitive experimental tool to distinguish between different anomalous-scattering-factor models.

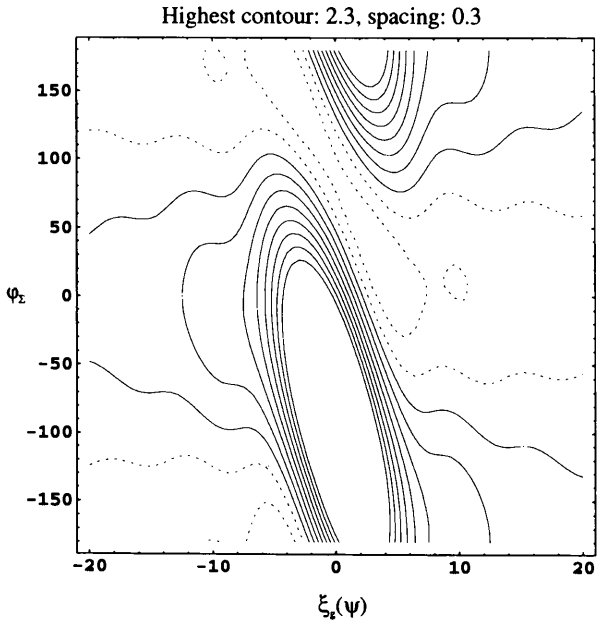

(*a*)

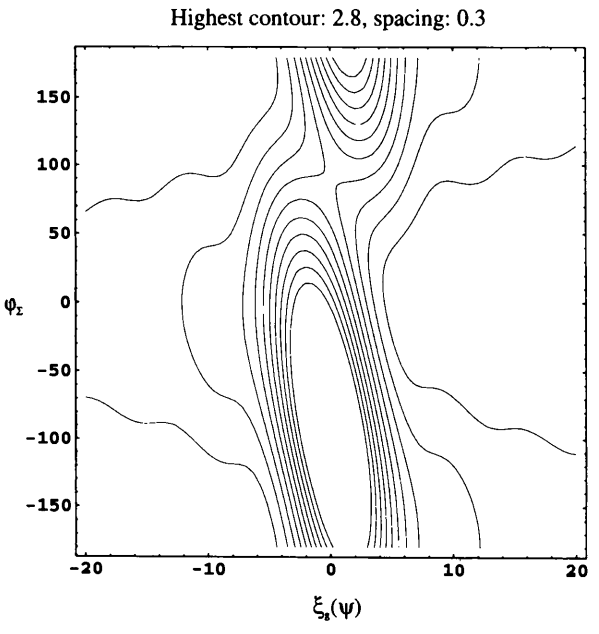

(*b*)

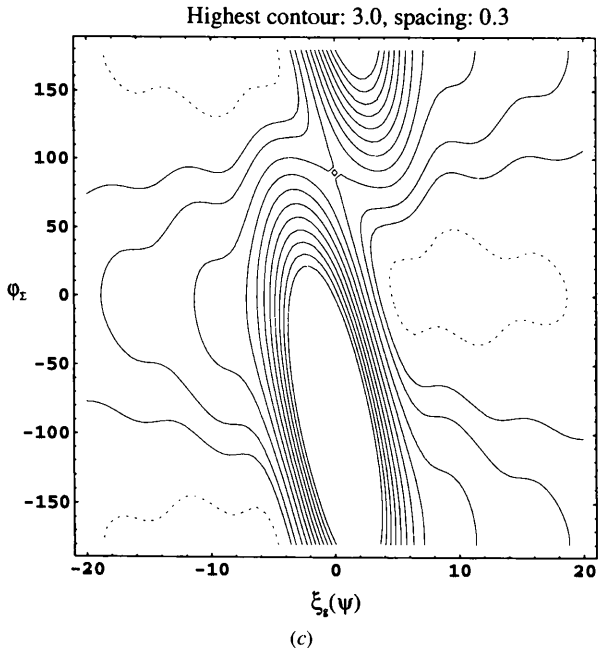

(*c*)

Fig. 5. Relative integrated power as a function of the invariant triplet phase sum and the normalized excitation error. Influence of incident-beam polarization. Laue–Laue case. (*a*) σ-polarized case, (*b*) π-polarized case, (*c*) unpolarized case. Model parameters used: $|\eta_{oh}^{\sigma\sigma}| = 0.050$, $|\eta_{oh}^{\pi\pi}| = 0.030$, $|\eta_{og}^{\pi\pi}| = 0.32$, $|\eta_{og}^{\pi\pi}| = 0.34$, $|\eta_{og}^{\pi\sigma}| = 0.030$, $|\eta_{gh}^{\sigma\sigma}| = 0.40$, $|\eta_{gh}^{\pi\pi}| = 0.42$, $|\eta_{gh}^{\sigma\pi}| = 0.050$. Dashed contours indicate negative values.

APPENDIX *A*

A1. The functions $\{g_i\}$

$$g_1(u) = [1 - \exp(-2u)]/2u$$

$$g_2(u, v) = [1 + \exp(-2v) - 2\exp(-v)\cos u]/(u^2 + v^2)$$

$$g_3(u, v) = (u^2 + v^2)^{-2}[-v^2 + v^3 + u^2 + u^2v - (u^2 - v^2) \times \exp(-v)\cos u - 2uv\exp(-v)\sin u]$$

$$g_4(u, v) = (u^2 + v^2)^{-2}[u(-2v + u^2 + v^2) + 2uv \times \exp(-v)\cos u + (-u^2 + v^2)\exp(-v)\sin u]$$

$$g_5(u, v) = [2v(u^2 + v^2)^2]^{-1}[-3v^2 + 2v^3 + u^2 + 2u^2v - (u^2 + v^2)\exp(-2v) + 4v^2\exp(-v)\cos u - 4uv\exp(-v)\sin u]$$

$$g_6(u) = [1 - (1 + 2u)\exp(-2u)]/4u^2$$

$$g_7(u, v) = (u^2 + v^2)^{-2}[v + (v + u^2 + v^2)\exp(-2v) - (2v + u^2 + v^2)\exp(-v)\cos u]$$

$$g_8(u, v) = (u^2 + v^2)^{-2}[u + u\exp(-2v) - 2u\exp(-v) \times \cos u - (u^2 + v^2)\exp(-v)\sin u]$$

$$g_9(u, v) = [4v(u^2 + 4v^2)^2]^{-1}[-12v^2 + 16v^3 + u^2 + 4u^2v - (u^2 + 4v^2)\exp(-4v) + 16v^2\exp(-2v) \times \cos u - 8uv\exp(-2v)\sin u]$$

$$g_{10}(u, v) = [4v(u^2 + 4v^2)^3]^{-1}[-u(u^2 + 4v^2)\exp(-4v) + u(-28v^2 + 16v^3 + 4u^2v + u^2) + 4uv(8v + u^2 + 4v^2)\exp(-2v)\cos u + 4v(4v^2 + 8v^3 - 3u^2 + 2u^2v) \times \exp(-2v)\sin u]$$

$$g_{11}(u, v) = [16v^2(u^2 + 4v^2)^3]^{-1}[-144v^4 + 128v^5 + 32u^2v^2 + 32u^2v^3 + u^4 - (u^2 + 4v^2)(12v^2 + 16v^3 + u^2 + 4u^2v)\exp(-4v) - 16v^2(-12v^2 - 8v^3 + u^2 - 2u^2v)\exp(-2v)\cos u - 16uv^2(8v + 4v^2 + u^2)\exp(-2v)\sin u].$$

A2. The coefficients $\{c_i\}$ *for symmetrical scattering*

For the actual scattering geometry, the coefficients $\{c_i\}$ may be given by

$$c_1 = \cos 2\theta_{oh}$$

$$c_2 = \cos \theta_{oh}$$

$$c_3 = \cos \varphi$$

$$c_4 = \sin \theta_{oh} \sin \varphi.$$

φ is the angle between $\hat{\mathbf{s}}_g$ and the normal to the plane spanned by $(\hat{\mathbf{s}}_o, \hat{\mathbf{s}}_h)$.

A3. The functions $\{f_i\}$

$$f_1(u) = (1/u^2)(1 - \cos u)$$

$$f_2(u) = (1/u)[1 - (1/u)\sin u]$$

$$f_3(u) = (1/u^2)[1 - (1/u)\sin u]$$

$$f_4(u) = (1/u^2)[\sin u - (2/u)(1 - \cos u)].$$

Parts of this work have been presented at the International School of Crystallography. 23rd Course: X-ray and Neutron Dynamical Diffraction: Theory and Applications, Erice, Italy, 1996.

References

Alexandropoulos, N. G., McWahn, D., Juretschke, H. J. & Kotsis, K. A. (1990). *Acta Cryst.* A**46**, C416.
Cannata, R., Martelli, S., Mazzone, G. & Sacchetti, F. (1989). *Acta Cryst.* A**45**, 679–686.
Caticha-Ellis, S. (1969). *Acta Cryst.* A**25**, 666–673.
Chang, S.-L. & Tang, M.-T. (1988). *Acta Cryst.* A**44**, 1065–1072.
Cromer, D. (1995). Private communication.
Cromer, D. & Liberman, D. (1970). *J. Chem. Phys.* **53**, 1891–1898.
Cromer, D. & Liberman, D. (1981). *Acta Cryst.* A**37**, 267–268.
Hümmer, K. & Weckert, E. (1994). Fifteenth European Crystallographic Meeting, Dresden, Germany. Abstracts, pp. 41–45.
Juretschke, H. J. (1982*a*). *Phys. Rev. Lett.* **48**, 1487–1489.
Juretschke, H. J. (1982*b*). *Phys. Lett.* A**92**, 183–185.
Juretschke, H. J. (1984). *Acta Cryst.* A**40**, 379–389.
Juretschke, H. J. (1986*a*). *Phys. Status Solidi B*, **135**, 455–465.
Juretschke, H. J. (1986*b*). *Acta Cryst.* A**42**, 449–456.
Kissel, L. (1995). Private communication.
Kissel, L., Pratt, R. H. & Roy, S. C. (1980). *Phys. Rev. A*, **22**, 1970–2004.
Kissel, L., Zhou, B., Roy, S. C., SenGupta, S. K. & Pratt, R. H. (1995). *Acta Cryst.* A**51**, 271–288.
Larsen, H. B. (1997). Doctoral thesis, The Norwegian University of Science and Technology, Trondheim, Norway.
Lipscomb, W. N. (1949). *Acta Cryst.* **2**, 193–194.
Luh, S.-W. & Chang, S.-L. (1991). *Acta Cryst.* A**47**, 502–510.
Moon, R. M. & Shull, C. G. (1964). *Acta Cryst.* **17**, 805–812.
Prager, P. R. (1971). *Acta Cryst.* A**27**, 563–569.
Schwegle, W., Hümmer, K. & Weckert, E. (1990). *Acta Cryst.* A**46**, C417.
Shen, Q. (1993). *Acta Cryst.* A**49**, 605–613.
Shen, Q. & Finkelstein, K. (1990). *Phys. Rev. Lett.* **65**, 3337–3340.
Thorkildsen, G. & Larsen, H. B. (1998). *Acta Cryst.* A**54**, 120–128.
Thorkildsen, G., Larsen, H. B., Mo, F., Semmingsen, D. & Mathiesen, R. H. (1998). In preparation.
Weckert, E. & Hümmer, K. (1997). *Acta Cryst.* A**53**, 108–143.